BULLETIN OF THE POLISH ACADEMY OF SCIENCES
TECHNICAL SCIENCES, Vol. 61, No. 2, 2013
DOI: 10.2478/bpasts-2013-0044

Load carrying capacity numerical study of I-beam pillar structure with blast protective panel

L. MAZURKIEWICZ*, D. KOLODZIEJCZYK, K. DAMAZIAK, J. MALACHOWSKI, M. KLASZTORNY, and P. BARANOWSKI

Department of Mechanics and Applied Computer Science, Military University of Technology, 2 Kaliskiego St., 00-908 Warsaw, Poland

Abstract. The paper presents numerical analyses aimed at preliminary assessment of the protective panel effectiveness, which task is to protect the elements of building structures against explosion. For the criterion of assessing the effectiveness of the panel the load capacity of the column made of steel I-beam was chosen. Ultimate force was determined by using advanced computational procedure, which consisted of four stages: preload, blast simulation, dynamic response and static analysis of deformed structure. Blast load was simulated using Lagrangian-Eulerian domain coupling. Results indicated that the application of the protective panel significantly reduces the plastic deformation of the structure.

Key words: FE analysis, blast protection, stability study.

1. Introduction

The motivation to undertake the work aimed to develop protective panels was described in [1], where it was pointed out that majority of terrorist attacks are mainly bombing attacks. The problem of blast wave interaction with a structure and its destructive effect has already been presented in many papers [2–4]. The previous research showed that dynamic response and the deformations of the base structure elements due to blast impact can be accurately predicted [5–6]. But the dynamic response of analysed element is insufficient to assess whole structure stability. The residual load carrying capacity of the supporting elements is critical for global stability as well as safety of the people inside the object. This parameter can be also a very effective tool to evaluate the protective panel effectiveness (crashworthiness).

The structural elements can resist the blast (no destruction occurs), but large deformation decreases the load capacity and that can cause the global collapse. Determination of the maximum axial load for the supporting structures also with imperfections is very common problem and can be easily solved using numerical methods or even analytically [9–11]. However it should be noticed that those procedure usually does not take into consideration the stresses after the blast, but only the geometrical imperfections (deformation).

The part of research presented in this paper is aimed at the advanced, multistage analysis procedure of determination of a support structure load capacity. This approach was presented in [10–12], but the procedure which was used by authors was very time consuming because the preload, blast and post-blast stages were calculated using the explicit code only.

2. Analysed problem

Geometry of the analysed structure is shown in Fig. 1. A support pillar is made of I-beam and is loaded by weight of a surrounding roof structure, represented by the force P and the lumped mass M. The multilayer protective panel consists of steel, fibre reinforced composite and metallic foam. A choice of such a layout was partially driven by experimental results showing a very good crashworthiness of foam and composites assembled together [13]. It is assumed, that two different phenomena are responsible for minimization of shock wave effects: flow around cylindrical panel and energy absorption by a panel structure. Mass of the charge was evaluated based on "abandoned briefcase" scenario, where a briefcase filled with TNT lies just near the pillar.

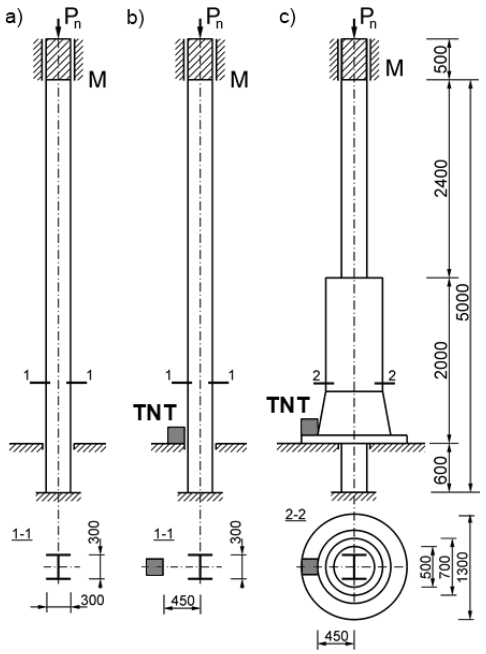

Fig. 1. Investigated problem a) perfect I-beam structure b) pillar subjected to blast wave and c) pillar with protective panel also subjected to blast wave [mm]

*e-mail: malachowskij@wat.edu.pl

From the analytical point of view, such scenario means that the blast wave is acting on the preloaded I-beam. It also means that static problems of preload and limit load investigation has to be separated by a highly dynamic outbreak event, which must be analysed using special numerical techniques. Therefore authors decided to use the commercial code LS-Dyna, which is particularly suited to a model such short, highly dynamic phenomena. The additional advantage of this choice was ability to chain different types of solvers/analyses implemented in the code. This allowed the running sequence of calculation using just one numerical model.

3. Numerical analysis

Evaluation of blast influence on load capacity of the investigated structure was carried out by comparison of results derived for three models: perfect I-beam structure, pillar subjected to blast acting directly and for pillar covered with protective panel. All three models were prepared using the same FE base model, by subtracting part of the model or by changing analysis sequence.

3.1. FE Model. FEM models of the column and each part of protective panel were developed. Part of the panel made from metallic foam was modelled using 8-node hex elements. Other parts of panel assembly, as well as a column were discretized using 4-node Belytschko-Lin-Tsay shell elements (Fig. 2).

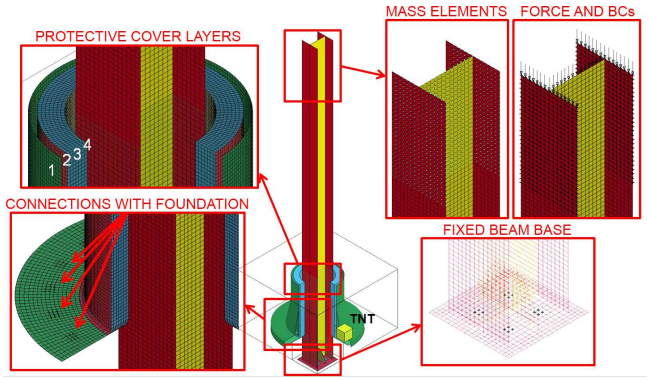

Fig. 2. FEM model of supporting beam with protective panel

Both the column and panel mount to a concrete foundation were modelled by fixing translational degrees of freedom in appropriate nodes. Additional rigid walls were also introduced to describe contact conditions between a concrete base and the structure. In order to save computer resources, fluid domain, required to model blast wave propagation, covered only a lower part of the panel and the post. Ready to run the FEM model consisted of 1.078 mln Euler (fluid) elements and over 78,000 Lagrange (structural) elements. The whole model is shown in Fig. 2.

3.2. Material model. A load due to outbreak causes very rapid changes of the strain field in the structure. Therefore, the elastic-plastic material model with isotropic hardening and strain rate effects was applied in order to describe properties of the beam material. Thus, simplified Johnson-Cook model was implemented, which provides a prediction of flow stress σ_{flow} for large strains and high strain rates, when its dependence on strain rate is linear in a semi logarithmic scale. The mathematical formula which describes this model is as follows [14]:

$$\sigma_{flow} = \left[A + B\left(\varepsilon^p\right)^n\right]\left(1 + C\ln\dot{\varepsilon}^p_*\right), \tag{1}$$

where A, B, C, n = material constants and $\dot{\varepsilon}^p_*$ = effective plastic strain rate (Table 1).

Table 1
Material properties for steel

ρ [kg/m^3]	A [MPa]	B [MPa]	C	n
7850	215	315	0.0936	0.9

To describe the composite elements behaviour the orthotropic material model with model failure mechanisms was applied. The various types of failure were specified in the model [14]:

- for the tensile fibre mode:

$$\sigma_{aa} > 0 \text{ then}$$
$$e_f^2 = \left(\frac{\sigma_{aa}}{X_t}\right)^2 + \beta\left(\frac{\sigma_{ab}}{S_c}\right)^2 - 1 \begin{cases} \geq 0 \text{ failed} \\ < 0 \text{ elastic} \end{cases} \tag{2}$$
$$E_a = E_b = G_{ab} = \nu_{ba} = \nu_{ab} = 0,$$

- for the compressive fibre mode:

$$\sigma_{aa} < 0 \text{ then } e_c^2 = \left(\frac{\sigma_{aa}}{X_c}\right)^2 - 1 \begin{cases} \geq 0 \text{ failed} \\ < 0 \text{ elastic} \end{cases} \tag{3}$$
$$E_a = \nu_{ba} = \nu_{ab} = 0,$$

- for the tensile matrix mode:

$$\sigma_{bb} > 0 \text{ then}$$
$$e_m^2 = \left(\frac{\sigma_{bb}}{Y_t}\right)^2 + \left(\frac{\sigma_{ab}}{S_c}\right) - 1 \begin{cases} \geq 0 \text{ failed} \\ < 0 \text{ elastic} \end{cases} \tag{4}$$
$$E_b = \nu_{ba} = 0 \;\rightarrow\; G_{ab} = 0,$$

- for the compressive matrix mode:

$$\sigma_{bb} < 0 \text{ then}$$
$$e_d^2 = \left(\frac{\sigma_{bb}}{2S_c}\right)^2 + \left[\left(\frac{Y_c}{2S_c}\right)^2 - 1\right]\frac{\sigma_{bb}}{Y_c} - 1 \begin{cases} \geq 0 \text{ failed} \\ < 0 \text{ elastic} \end{cases} \tag{5}$$
$$E_b = \nu_{ba} = \nu_{ab} = 0 \;\rightarrow\; G_{ab} = 0,$$

where a – fibre direction, b – crossfibre direction, X_t, X_c – tensile (t) and compressive (c) strength in direction a, Y_t, Y_c – tensile (t) and compressive (c) strength in direction b, S_c – shear strength.

If the criterion is reached the corresponding values of parameters (pointed above) are reduced to zero.

In the material model also erosion can occurs when:

- the tensile fibre strain is greater than $\varepsilon^+_{\max}$ (maximum strain for fibre tension) or smaller than $\varepsilon^-_{\max}$ (maximum strain for fibre compression),

- the effective strain is greater than ε_{fs} (effective failure strain).

When failure has occurred in all of the composite layers (through-thickness integration points), the element is deleted.

Another important component of the panel is a metallic foam applied to consume the blast wave energy by the plastic deformation. The behaviour of that material was described by the honeycomb material model. In this model the elastic moduli vary, from their initial values to the fully compacted values at V_f, linearly with the relative volume V. The relative volume, V, is defined as the ratio of the current volume to the initial volume. Typically, $V = 1$ at the beginning of a calculation. For the uncompacted material, the trial stress components are updated using the elastic interpolated moduli [14]:

$$\sigma_{ij}^{n+1\,trial} = \sigma_{ij}^{n} + E_{ij}\Delta\varepsilon_{ij}. \tag{6}$$

When stress values exceed the permissible values determined from the material curves then we have:

$$\sigma_{ij}^{n+1} = \sigma_{ij}(V)\frac{\lambda\sigma_{ij}^{n+1\,trial}}{\left|\lambda\sigma_{ij}^{n+1\,trial}\right|}, \tag{7}$$

where λ is a parameter in function of strain-rate defined by curve.

For a fully compacted material it is assumed that the material behaviour is elastic-perfectly plastic and the stress components updated according to:

$$\sigma_{ij}^{trial} = \sigma_{ij}^{n} + 2G\Delta\varepsilon_{ij}^{dev\,n+1/2}, \tag{8}$$

where $\Delta\varepsilon_{ij}^{dev\,n+1/2}$ is deviatoric strain increment.

The material properties for composite (Table 2) and metallic foam were obtained from experimental tests.

Table 2
Material properties for composite material

ρ [kg/m^3]	E_a [MPa]	E_b [MPa]	ν_{BA}	G_{AB} [MPa]
1800	22050	6765	0.099	3200
G_{BC} [MPa]	G_{CA} [MPa]	X_c [MPa]	X_t [MPa]	Y_c
1670	3200	375	402	110
Yt [MPa]	S_c [MPa]	$\varepsilon^{-}_{\max}$	$\varepsilon^{+}_{\max}$	ε_{fs}
34.4	45.8	−0.02	0.02	0.05

3.3. Analysis procedure. Investigation of the perfect structure load capacity required only one, static step. For two other cases, simulation was divided to four stages (Fig. 3).

In the first stage I-beam structure was subjected to nominal load P_n, which was equal to the load carried by the pillar during its normal service. An incremental static analysis was performed using the full Newton-Rapshon algorithm. Equation solved in this stage had the following form:

$$K_i\Delta x_{i-1} = \Delta Q_i, \tag{9}$$

where K_i – stiffness matrix, Δx_{i-1} – displacement vector, ΔQ_i – external force vector.

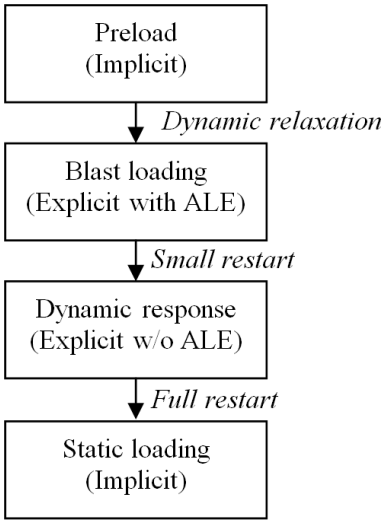

Fig. 3. Analysis procedure scheme

Convergence of the problem was controlled by two criteria: displacement relative convergence tolerance and energy relative convergence tolerance.

In the second stage results from the previous stage were taken into account as pre-stress field presented in the column. It was obtained by using dynamic relaxation procedure. Dynamic relaxation allows for quickly reaching preloaded state by linear ramping nodal displacement field to prescribed values over 100 time steps. It should be noticed that the comparison of the stress field taken from static analysis and stress field generated by dynamic relaxation procedure showed small differences introduced by the latter. On the other hand, the procedure allows for application of predefined stress filed on selected part of FE model in a very effective manner.

The blast loading in this stage required to apply transient dynamics procedure with explicit central difference time integration. Equation solved had the following form:

$$M\ddot{x}_n = F_n^{ext} - F_n^{int} - C\dot{x}_n, \tag{10}$$

where M – the diagonal mass matrix, F_n^{ext} – external and body force loads, F_n^{int} – the stress divergence vector, C – dumping matrix.

Gas domain, consisted of air and detonation products, was modelled using finite volume technique (so called Euler formulation). The coupling between Lagrangian formulation (solid material) and Eulerian formulation (gas medium) was taken into account during calculations. Generally *ALE* procedure consists of the following sequence of steps: the classical Lagrangian step and the advection step. The advection step is carried out with the assumption that changes in the positioning of nodes are only slight (very small) in comparison to characteristics (lengths of elements that surround these nodes).

In the performed numerical tests the detonation process of *TNT* high explosive material was implemented through the automatically programmed burn model, supported by LS-DYNA

using so called the "explosive burn" material model. The energy contained in the *HE* was assumed to be immediately released inside the front of a detonation wave. The detonation requires modelling of the movement of the *PD* (product of detonation) after reaching successive locations by the *DW* (detonation wave) front. Hence the Jones-Wilkins-Lee (*JWL*) equation of a state was implemented in the applied explosive burn model with the following form [14, 15]:

$$p = A\left(1 - \frac{\omega}{R_1\overline{\rho}}\right)\exp\left(-R_1\overline{\rho}\right) + B\left(1 - \frac{\omega}{R_2\overline{\rho}}\right)\exp\left(-R_2\overline{\rho}\right) + \frac{\omega\overline{e}}{\overline{\rho}}, \tag{11}$$

where $\overline{\rho} = \rho_{HE}/\rho$; $\overline{e} = \rho_{HE}e$; ρ_{HE} – density of the high explosive; p – pressure of *PD*; e – specific internal energy of *PD* and ρ – density of *PD*. A, B, R_1, R_2, ω are empirical constants determined for specific type of a high explosive. All constants required (Table 3) are taken from literature [5]. A typical pressure time history is presented in Fig. 4 [16].

Table 3
Material properties for HE [5]

ρ_{HE} [kg/m^3]	A [GPa]	B [GPa]	R_1	R_2	ω
1630	373.8	3.747	4.15	0.9	0.35

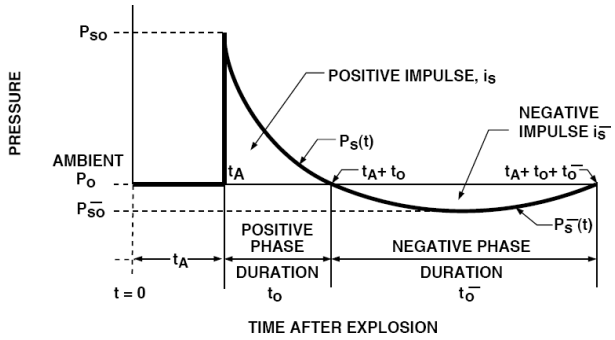

Fig. 4. Typical pressure-time history of pressure wave from explosion after Ref. [16]

In the following stage, I-beam response to the blast wave was assessed. The main difference between the previous stage was that the sole interest was only the pillar without other parts. Therefore, so called "small restart" was used to remove the Euler domain as well as a panel structure, together with yhe corresponding contact and FSI interfaces from the numerical model. This allowed to reduce the FE model size to 12 K elements (almost 100 times less than in the full model) and thus, to increase time covered by an analysis and to shrink wall time required for computations. The termination time of the analysis was the moment at which further growth in plastic deformation could not be observed.

The final stage was similar to the first one in terms of analysis type. Again the static analysis with the Newton-Raphson procedure was used. However, this time, data exchange required to generate pre-stress state in the I-beam, was conducted using more accurate "stress initialization" option. The convergence was based on relative displacement (0.001) and energy (0.01) norm with minimum allowed load step equals 0.001 of the nominal load. Structure was loaded by a multiple of operating force, so that the iteration procedure could reach the point of divergence due to the ill-conditioned stiffness matrix. A load value causing divergence conditions was considered as the load capacity of the structure. It should be pointed out that due to the chosen algorithm (Newton-Raphson) this is the approximate value of force. At this stage of analysis with a preloaded structure it was impossible to use the arc length method.

4. Analysis results

In Fig. 5 axial, vertical force vs. axial, vertical deflection are shown. The blast wave effects can be clearly seen as shift of the displacement value (at the nominal force value). It can also be noticed that the protection panel works correctly (reduces the structure deformation), although does not provide full protection (blast wave reached the structure). The amount of energy absorbed by the pillar is significantly smaller (Fig. 6).

For better and clearer presentation, results shown in Fig. 5 were normalized, so displacement axis starts after third analysis stage (Fig. 7). It can be interpreted as investigation of a limit load value for the perfect structure (no blast) and for two other perturbed geometries, where imperfections level depends on protective panel occurrence. Results show, that although the protected column suffered from plastic deformation (imperfections), it can virtually carry the same load as unperturbed geometry. High deformations of the structure without panel reduce the load carrying capacity, but for this particular setup (pillar section, boundary conditions, charge weight and location) the pillar can still support almost 90% of the load carried by the perfect unperturbed structure. In Fig. 8 final deflection of a beam axis for all three geometries is shown. The area affected by blast wave dominates in the case of the unprotected structure. On the deflection curve of protected column effects of outbreak are also noticeable, but it has rather local character. Therefore global structure behaviour is similar to elastic beam.

The protective panel influence can be much more clearly noticed in Fig. 9, where plastic strain distributions are shown for protected and unprotected I-beam structure.

For the investigated mass and location of charge, blast wave impact generated well developed plastic deformations in the unprotected structure (close to ultimate strains), while the protected structure remained virtually elastic.

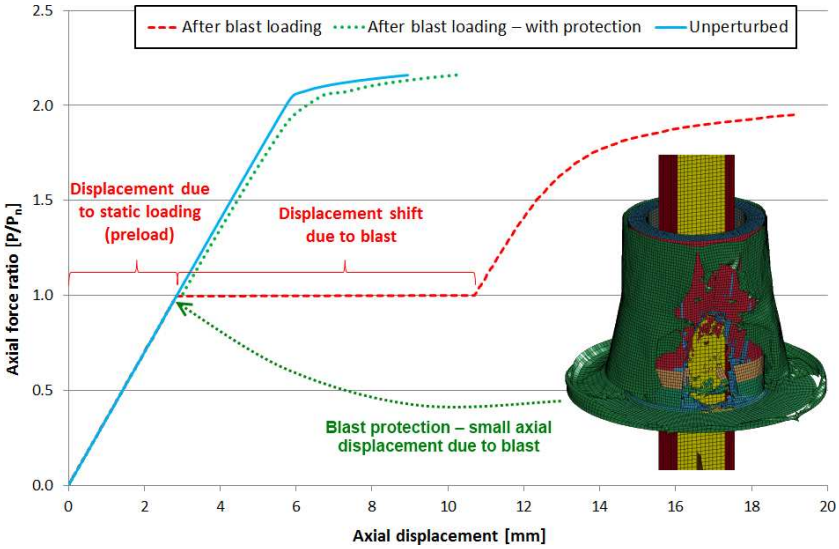

Fig. 5. Axial force versus axial displacement of supporting beam

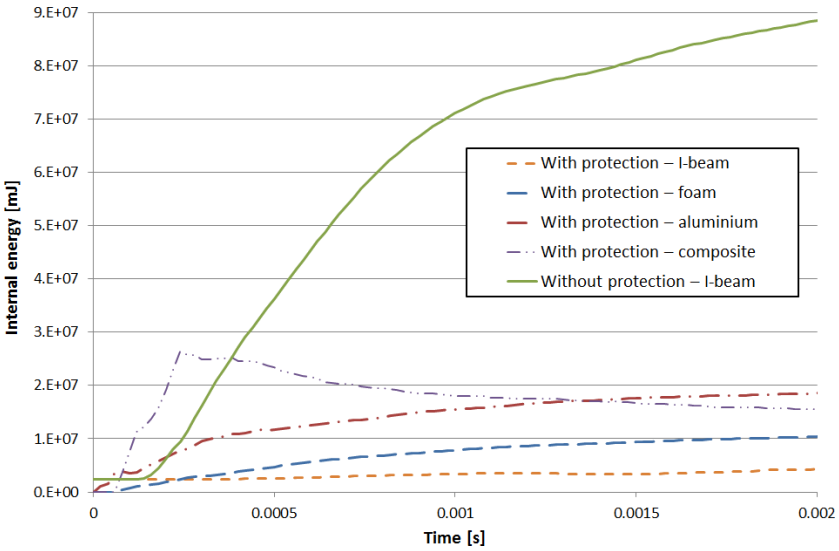

Fig. 6. Internal energy during the blast stage

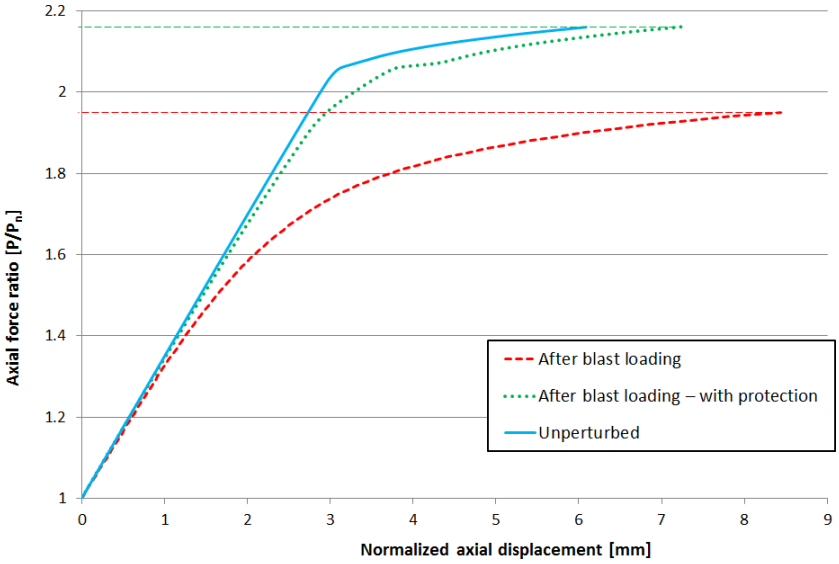

Fig. 7. Axial force versus normalized axial displacement of supporting beam

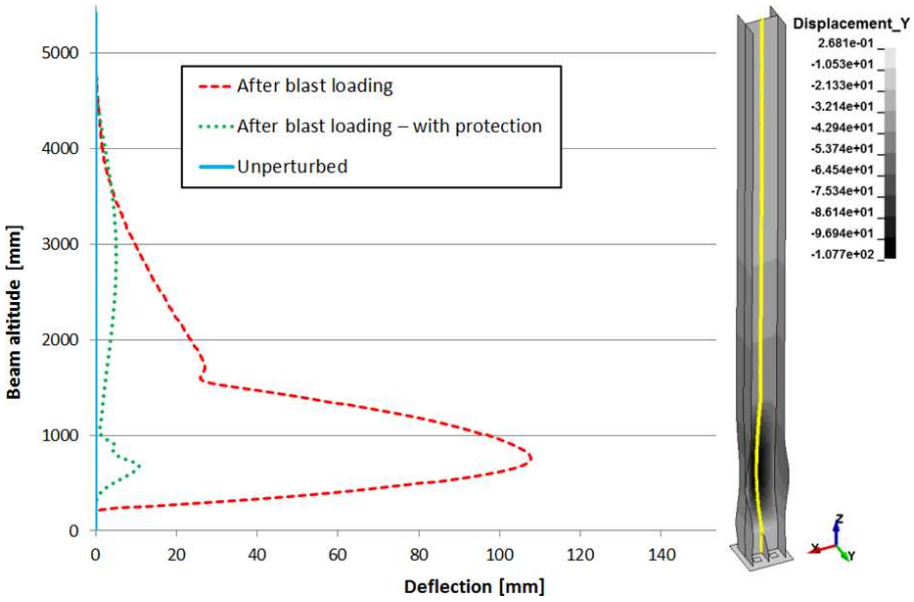

Fig. 8. Deflection profile of supporting beams

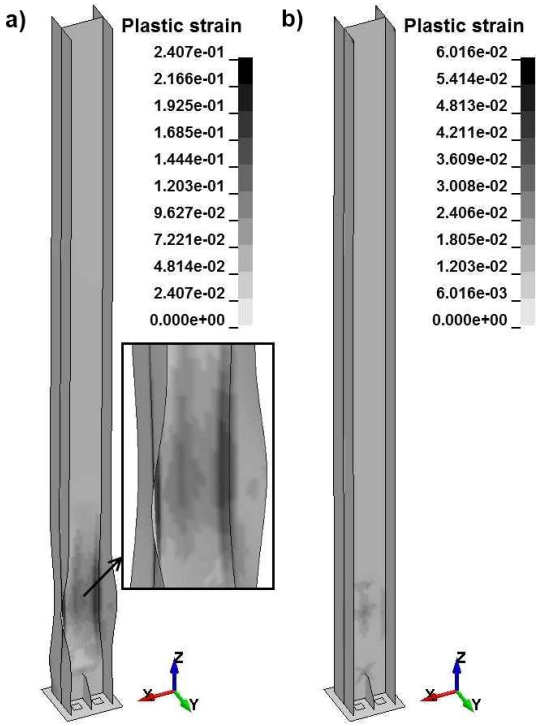

Fig. 9. Plastic strain of deformed pillar a) without protection and b) with protection

5. Conclusions

The developed multistage analysis allowed to investigate such a complex problem which could not be analysed using only one numerical technique. Preload and stabilization after outbreak are simply time-consuming to be covered by an explicit algorithm. On the other hand, a static procedure does not allow for simulating the blast wave at all. It can be stated, that chaining different procedures is the only way to include imperfection due to blast wave in the analysis.

The investigated beam structure is very resistant, compared to predicted service loading. Therefore, influence of imperfections caused by the blast wave on maximum carrying load is not very obvious. For this particular setup, despite the strains they almost reach the ultimate limit, the pillar load carrying capacity does not decrease significantly.

Finally the very important role of the protective panel in the analysed problem is simply to prevent the placement of the charge close to the structure and consume the blast wave energy in order to avoid the structure failure due to plastic deformations. However the reduction of a load carrying capacity due to deformations after the outbreak can be very significant for different set-up of a pillar section and a charge shape, weight or location and should be carefully investigated. The presented procedure is a very efficient way to determine the load carrying capacity and can be simply introduced to blast response analyses.

Acknowledgements. The research was carried out under a research grant from the Polish Ministry of Science and Higher Education no. 0097/R/T00/2010/12. This support is gratefully acknowledged.

REFERENCES

[1] Ł. Mazurkiewicz and J. Małachowski, "Analysis of selected structural components subjected to blast wave", *J. KONES Powertrain and Transport* 19 (1), 267–272 (2012).

[2] L.A. Louca and R.M. Mohamed Ali, "Improving the ductile behaviour of offshore topside structures under extreme loads", *Eng. Structures* 30, 506–521 (2008).

[3] E. Tang and H. Hao, "Numerical simulation of a cable-stayed bridge response to blast loads, Part I: Model development and response calculations", *Eng. Structures* 32, 3180–3192 (2010).

[4] Y. Lu and Z. Wang, "Characterization of structural effects from above-ground explosion using coupled numerical simulation", *Computers and Structures* 84, 1729–1742 (2006).

[5] J. Malachowski, *Modelling and Testing on Interaction of Solid Body-Gas at the Pressure Impulse Influence on Elements of Pipeline*, BEL Studio, Warszawa, 2010, (in Polish).

[6] J. Malachowski, "Influence of HE location on elastic-plastic tube response under blast loading", *Shell Structures Theory and Applications* 2, 179–182 (2010).

[7] M. Arif Gurel, R. Kadir Pekgokgoz, and F. Cili, "Strength capacity of unreinforced masonry cylindrical columns under seismic transverse forces", *Bull. Earthquake Eng.* 10, 587–613 (2012).

[8] S. Machado, "Non-linear stability analysis of imperfect thin-walled composite beams", *Int. J. Non-Linear Mechanics* 45, 100–110 (2010).

[9] Y. Liu and L. Gannon, "Finite element study of steel beams reinforced while under load", *Engineering Structures* 31 (11), 2630–2642 (2009).

[10] K. Wu, B. Li, and K. Tsai, "The effects of explosive mass ratio on residual compressive capacity of contact blast damaged composite columns", *J. Constructional Steel Research* 67, 602–612 (2011).

[11] X. Bao and B. Li, "Residual strength of blast damaged reinforced concrete columns", *Int. J. Impact Eng.* 37, 295–308 (2010).

[12] R. Jayasooriya, D.P. Thambiratnam, N.J. Perera, and V. Kosse, "Blast and residual capacity analysis of reinforced concrete framed buildings", *Engineering Structures* 33, 3483–3495 (2011).

[13] S. Ochelski, P. Bogusz, and A. Kiczko, "Static axial crush performance of unfilled and foamed-filled composite tubes", *Bull. Pol. Ac.: Tech.* 60 (1), 31–35 (2012).

[14] J.O. Hallquist, *LS-Dyna. Theory Manual*, Livermore Publishing House, Livermore, 2006.

[15] E. Wlodarczyk, *Fundamentals of Detonation*, Military University of Technology, Warsaw, 1995.

[16] "Unified Facilities Criteria (UFC) structures to resist the effects of accidental explosions", *U.S. Army Corps of Engineers, UFC* 3-340-02, (2008).